Solid State Communications 167 (2013) 27–30

Contents lists available at SciVerse ScienceDirect

Solid State Communications

journal homepage: www.elsevier.com/locate/ssc

Electronic properties of carbon nanotubes partially unzipped by oxygenation or fluorination

Gunn Kim [a,*], Hyung-June Lee [b], Young-Kyun Kwon [b]

[a] Department of Physics and Graphene Research Institute, Sejong University, Seoul 143-747, Republic of Korea
[b] Department of Physics and Research Institute for Basic Sciences, Kyung Hee University, Seoul 130-701, Republic of Korea

ARTICLE INFO

Article history:
Received 6 February 2013
Received in revised form
29 April 2013
Accepted 3 June 2013
by D.D. Sarma
Available online 12 June 2013

Keywords:
A. Unzipping
A. Carbon nanotubes
D. Band structure
E. First-principles calculations

ABSTRACT

Unzipping carbon nanotubes has recently attracted interest as a promising route to synthesizing semiconducting graphene nanoribbons. Here, the band structures of O- and F-driven partially unzipped armchair carbon nanotubes (PUCNTs) are computed using the *ab initio* pseudopotential method. Although the model structures exhibit a similar pinhole with a length of ~1 nm along the tube axis, the band structures differ distinctly. The O-driven PUCNT has many localized states in the valence band arising mainly from the O 2*p* orbitals, and preserves metallic properties. In contrast, the F-driven PUCNT shows properties of a semiconductor with a bandgap of ~0.15 eV, and its localized states occur in the conduction band. When the unzipping process continues further, the O-driven PUCNT also shows the semiconducting behavior.

1. Introduction

Graphene, a one-atom-thick hexagonal carbon layer, is one of the most fascinating materials explored for both fundamental studies and nanoelectronics application because of its unusual physical and chemical properties [1–5]. Future applications of graphene might include high-speed transistors and logic circuits. However, the main limitation in using graphene in nanoelectronics is its vanishing bandgap. Therefore, alternative materials such as graphene nanoribbons (GNRs) are explored for use in nanoelectronics. GNRs are advantageous as they have been predicted and confirmed experimentally to behave like semiconductors [6,7]. However, efforts to obtain narrow GNRs from larger graphene sheets using chemical methods have proven ineffective since wide GNRs (a few hundred nanometers in width) were produced by the methods.

Interestingly, ways to "unzip" carbon nanotubes (CNTs) to produce narrow GNRs were developed in 2009 [8–10]. Kosynkin et al. adopted wet chemical methods to break carbon–carbon bonds using potassium permanganate ($KMnO_4$) and sulfuric acid (H_2SO_4) as oxidizing agents, thereby unrolling the tubes along a single axis [8]. However, their GNRs, a few hundred nanometers in width, were not semiconducting. In contrast, Jiao et al. used ionized argon gas to etch away strips of CNTs in a polymer matrix [9]. The resulting GNRs were narrower, *i.e.*, about 10–20 nm wide. Other efficient methods for producing GNRs were also developed by many researchers. Cano-Márquez et al. employed longitudinal dissection of multi-walled nanotubes to form GNRs by treatments in liquid ammonia (NH_3) and lithium with subsequent exfoliation using hydrochloric acid and heat treatment, which is suitable in case of mass production [10]. Unzipped CNTs can also be produced through fluorination because fluorine is one of the strongest oxidizing agents. It has been shown that a high density of fluorine can be covalently attached to CNTs [11,12], which enhances their solubility [13]. In extreme cases, the tubes were found to be destroyed (i.e., unzipped) [11], as confirmed using transmission electron microscopy. Because a partially open CNT comprises both a CNT and a curved GNR, it is expected to have more diverse properties [14]. Recently, Li et al. treated multi-walled CNTs in a chemical solution and revealed that the outer walls partially opened to form nanosized graphene regions that clung to the inner wall, remaining mostly intact [15].

In this study, we compare the structural and electronic properties of oxygen- and fluorine-driven partially unzipped carbon nanotubes (PUCNTs) and elucidate the emergence of semiconducting behavior by investigating the structural and electronic properties of PUCNTs. Our density functional theory calculations reveal that the fluorinated system exhibits a bandgap with localized states in the conduction band, which is a prerequisite for future semiconducting devices.

2. Computational methods and model structures

We chose a (5, 5) CNT as a model system utilizing a simple tetragonal unit cell with periodic boundary conditions. The size in the tube axis direction was 26.1 Å, and the size in the lateral

* Corresponding author. Tel.: +82 2 3408 3968; fax: +82 2 3408 4316.
E-mail addresses: gunnkim@sejong.ac.kr, kimgunn@gmail.com (G. Kim).

0038-1098/$ - see front matter © 2013 Published by Elsevier Ltd.
http://dx.doi.org/10.1016/j.ssc.2013.06.001

direction of the supercell was 20 Å to avoid the spurious interactions between the neighboring supercells. Geometry optimizations employed convergence thresholds of 10^{-8} E_h and 10^{-4} E_h/a_B for the energies and forces, respectively. Here, $E_h \approx 27.2$ eV and $a_B \approx 0.529$ Å.

For the computations, we employed density functional theory with a Ceperley–Alder-type [16] exchange–correlation functional within the local density approximation (LDA). The basis set comprised a linear combination of localized pseudo-atomic orbitals [17] and Troullier–Martins-type norm-conserving pseudopotentials [18] with partial core corrections [19] to describe valence and core electrons, respectively, as implemented in the OpenMX package [20]. The pseudo-atomic orbitals were C5.0-s2p2, O5.0-s2p2, and F5.5-s2p2. The Brillouin zone was sampled with a $1 \times 1 \times 6$ irreducible Monkhorst–Pack k-point grid [21], and the energy cutoff for the real space mesh was 150 Ry.

3. Results and discussion

We first discuss the O-driven PUCNT. According to our calculations, a carbon–oxygen bond length is 1.23 Å, which can be assumed to be a double bond because the C–O bond length in an acetone molecule, $(CH_3)_2CO$, is 1.21 Å. This result indicates that the carbonyl (C=O) groups exist at the pinhole of the CNT. Since ketones have a carbonyl group bonded to two other carbon atoms, the O-driven PUCNT is a ketone. Ketones participate in many organic reactions, and so the O atoms in the O-driven PUCNT may be reactive. In addition, the CNTs become hydrophilic due to oxygenation since the terminated O atoms can make hydrogen bonds with water molecules. As shown in Fig. 1, the C1–C3 bond length and the C1–C2 distance are 1.44 Å and 10.50 Å, respectively. It is assumed that the attack of oxygen opens a pinhole of 3.13 Å in width (perpendicular to the tube axis). The O1–O3 (O2–O4) distance is 2.55 Å (2.57 Å), whereas the O1–O2 distance is 2.78 Å. The opening of the CNT due to oxygen adsorption results in the deformation of the CNT. Finally, the cross section of the CNT is elliptical (see Fig. 3). Our results are similar to those obtained in a previous study by Rangel et al. [22]. However, we placed all the pairs of oxygen atoms on the CNT at the same time for the geometry optimization, as opposed to their work, where pairs of oxygen atoms were added sequentially. Therefore, our relaxed structures are symmetric while those of Rangel et al. are not. In real experiments, the oxygen atoms would probably be attached sequentially onto the CNT surface and thus asymmetrically unzip it instantaneously. However, the PUCNT would be eventually symmetric since it is energetically more stable than its asymmetric

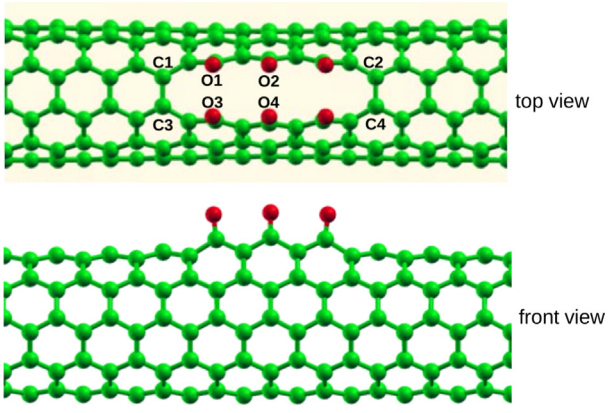

Fig. 1. (Color online) Optimized geometry of an oxygen-driven PUCNT. Three pairs of oxygen atoms are added and open the CNT in our model.

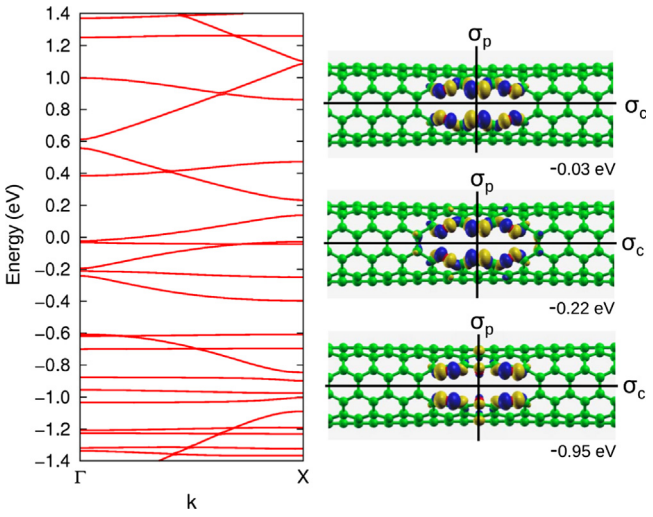

Fig. 2. (Color online) Electronic band structure of a oxygen-driven PUCNT and the wave functions of three localized states near the Fermi Level. The Fermi level is set to zero. The values for the yellow and blue isodensity surfaces are $\pm 0.03\ e/a_B^3$ where the sign is that of the wave function.

counterparts. In our calculations, therefore, we considered the symmetric PUCNT models.

Next, we calculated the electronic band structure and wave functions of an O-driven PUCNT; the results are shown in Fig. 2. Interestingly, this partially unzipped (5, 5) CNT maintains metallic properties. Here, we note that the defect-free armchair CNT is metallic. The O-driven PUCNT preserves two mirror (reflection) symmetry planes. One plane (σ_p) is perpendicular to the nanotube axis, and the other (σ_c) contains the tube axis, as shown in Fig. 2. As in bulk semiconductors, the localized states, introduced by the unzipping of the CNT, may act as scattering centers for charge carriers, thus significantly affecting the transport of CNTs. Therefore, we examined the localized states in the open part. The wave functions corresponding to the localized states at −0.05 eV, −0.22 eV, and −0.95 eV are antisymmetric, antisymmetric, and symmetric with respect to σ_c and antisymmetric, symmetric, and symmetric with respect to σ_p, respectively. Fig. 2 clearly shows that the electronic density of the third state ($E = -0.95$ eV) is smaller at the center of the open part. We expect that the conductance of the O-driven PUCNT may be greatly affected by the localized states at −0.05 eV and −0.22 eV. The three localized states arise mainly from the O $2p$ orbitals at the pinhole.

Fig. 3 shows a two-dimensional map of the electric potential of the O-driven PUCNT. In the open part, the dark blue and green colors represent the lower and higher potentials, respectively. The electric field is weak in regions where the spacing of equipotential lines is wide. Compared with the defect-free (5, 5) CNT, the band structure of the PUCNT changes because the potential affecting the electrons is severely deformed.

Now, we turn to the F-driven PUCNT. According to our calculation, the C–F bond lengths are 1.33 Å and 1.40 Å at the center and at the edge of the open part, respectively. In the case of fluorobenzene, the C–F bond length is ≈1.35 Å. Thus, the C–F bond lengths in the F-driven PUCNT are somewhat longer than that of the single bond at the edge of the open part. As depicted in Fig. 4, the C1–C3 bond length of 1.50 Å is comparable to that of a single carbon–carbon bond (1.54 Å); the C1–C2 distance is 10.54 Å. Because of the opening of the CNT due to the attacking fluorine atoms, a pinhole of 3.13 Å in width (perpendicular to the tube axis) is formed. The F1–F3 (F2–F4) distance is 2.51 Å (2.27 Å), whereas the F1–F2 distance is 2.81 Å. Here, an interesting finding is that the F1–F3 distance is a little longer than the F2–F4 distance. The top view of the model structure in Fig. 4

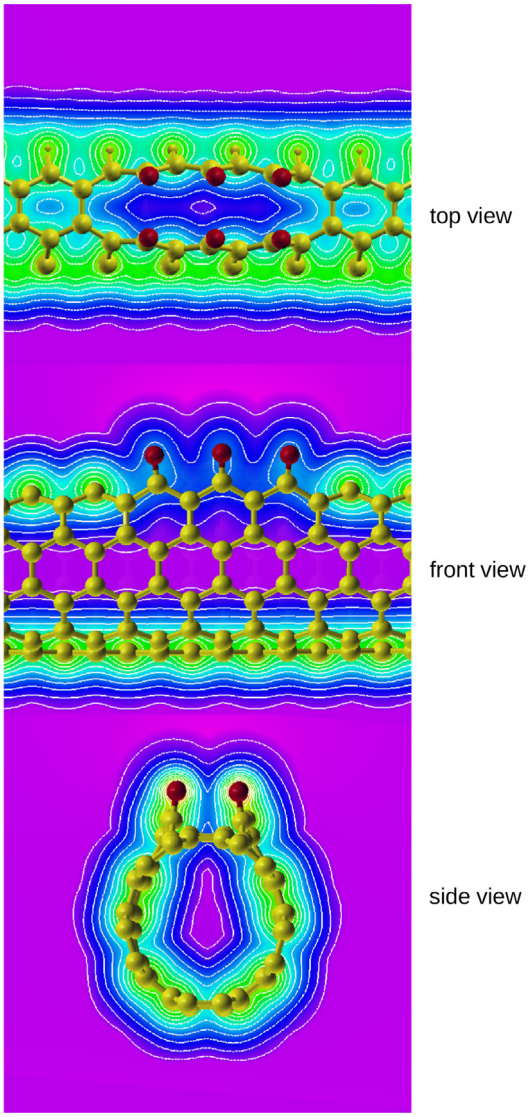

Fig. 3. (Color online) Two-dimensional map of the electric potential in the O-driven PUCNT. In the region near the ripped side wall, the electric potential is weaker than in other parts. The dark blue and green colors represent the lower and higher potentials, respectively.

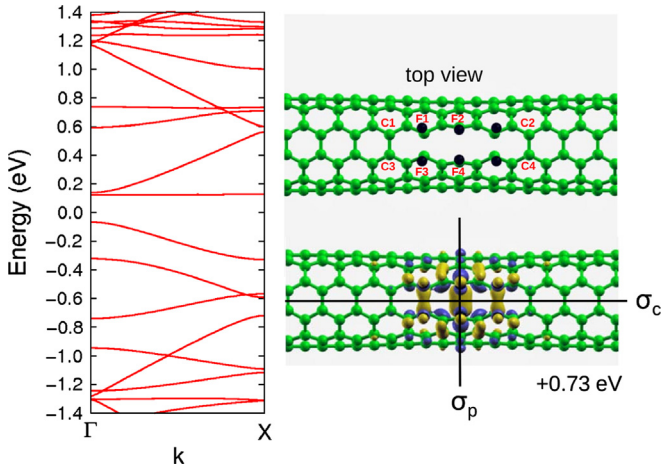

Fig. 4. (Color online) Optimized geometry of a fluorine-driven PUCNT, its electronic band structure and the wave function of a localized state in the conduction band. The Fermi level is set to zero. The values for the yellow and blue isodensity surfaces are $\pm 0.03\ e/a_B^3$.

shows that the C–F bonds are not parallel along the longitudinal direction, chiefly to avoid repulsion between F atoms [23]. Similar to the O-driven PUCNT, the F-driven one also undergoes radial deformation. The formation of C–F bonds impairs the π bonds in the CNT and changes the orbital hybridization of carbon from sp^2 to sp^3, thus distorting the local geometry [23].

As shown in Fig. 4, our model of the F-driven PUCNT exhibits semiconducting properties, and its energy bandgap is ~0.15 eV, which is in sharp contrast to the metallic O-driven PUCNT. Many flat bands originating from the O 2*p* orbitals in the valence band and at the Fermi level are found for the O-driven PUCNT (Fig. 2). Especially, the O 2*p* orbitals in the O-driven PUCNT are almost parallel to the axial direction between −1.4 and +1.4 eV. In contrast, the F 2*p* orbitals in the F-driven PUCNT are perpendicular to the axial direction and localized defect states occur mainly in the conduction band between −1.4 and +1.4 eV. Such a difference in the orientation of 2 *p* orbitals of the O and F atoms may be associated with the metal/semiconductor properties. The wave function corresponding to the localized state around the open part at +0.73 eV is symmetric with respect to σ_c and σ_p. For the localized state, the electron clouds connecting the C atoms bonded to the F atoms are inside the nanotube, and they are perpendicular to the tube axis. On the other hand, the electron densities derived from the F atoms are relatively small. Fig. 4 shows that the F 2*p* orbitals are parallel to the normal vector of the nanotube surface in the radial direction. Although a shallow defect level exists at +0.12 eV, its localization character is very weak.

Finally, we calculated a PUCNT with a larger unit cell (~4 nm) along the axis in order to investigate the supercell size effect. The change in the bond length is less than 7%, compared with the structures with the smaller supercell. Although the energy levels of the localized states are changed, the O-driven PUCNT is still metallic and the F-driven PUCNT is semiconducting with a bandgap of ~0.15 eV. In addition, we considered another unzipped configuration with a larger pinhole size for the larger unit cell of ~4 nm in the longitudinal direction. Fig. 5 shows that the PUCNT is a semiconductor with a bandgap of ~20 meV when five C–C bonds are broken by oxygenation. If the pinhole size in the longitudinal direction is longer, the PUCNT will be a semiconductor with a larger energy gap.

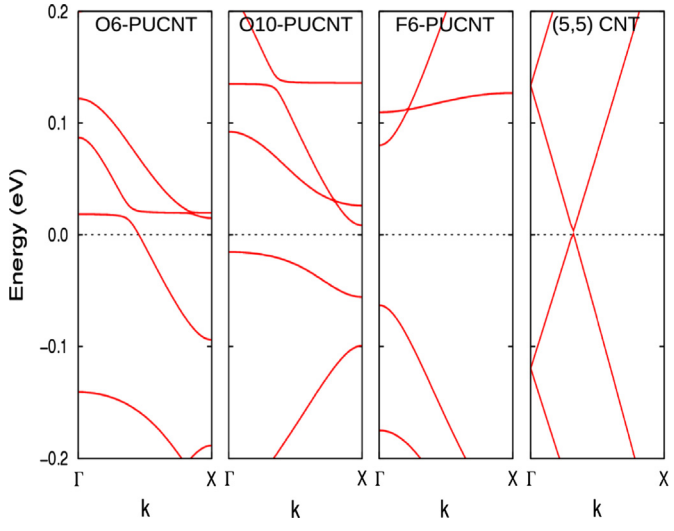

Fig. 5. (Color online) Electronic band structures of our models with a larger unit cell (~ 4 nm) along the axis. The O-driven PUCNT maintains metallic characteristics and the F-driven PUCNT preserves a bandgap of ~0.15 eV although the unit cell increases. When ten oxygen atoms are attached on the CNT, five carbon–carbon bonds are broken and the energy bandgap opens (the gap of ~20 meV).

4. Conclusion

In summary, we have compared the structural and electronic properties of O- and F-driven partially unzipped CNTs on the basis of first-principles calculations. For a (5, 5) carbon nanotube possessing a small pinhole with a length of ~1 nm along the tube axis, the band structures revealed that partial oxygenation preserved the metallic properties. The valence band exhibited many nearly flat bands, of which the least dispersive mainly arose from the O 2*p* electrons. When the size of the pinhole increases, the system becomes finally semiconducting. In contrast, the F-driven PUCNT with a similar pinhole size (~1 nm) gave rise to a bandgap opening. In this case, the flat bands are located in the conduction band. Consequently, one can expect that strong reflection occurs in the valence band, particularly just below the Fermi level, due to the localized states of the O-driven PUCNT. However, for the F-driven PUCNT, strong reflection could be observed mostly in the conduction band.

Acknowledgments

The authors thank Jiyoung Kim for fruitful discussions. This work was supported by the faculty research fund of Sejong University in 2011.

References

[1] P.R. Wallace, Phys. Rev. 71 (1947) 622.
[2] K.S. Novoselov, A.K. Geim, S.V. Morozov, D. Jiang, M.I. Katsnelson, I.V. Grigorieva, S.V. Dubonos, A.A. Firsov, Nature 438 (2005) 197.
[3] Y. Zhang, Y.-W. Tan, H.L. Stormer, P. Kim, Nature 438 (2005) 201.
[4] A.H. Castro Neto, F. Guinea, N.M.R. Peres, K.S. Novoselov, A.K. Geim, Rev. Mod. Phys. 81 (2009) 109.
[5] S. Das Sarma, S. Adam, E.H. Hwang, E. Rossi, Rev. Mod. Phys. 83 (2011) 407.
[6] K. Nakada, M. Fujita, G. Dresselhaus, M.S. Dresselhaus, Phys. Rev. B 54 (1996) 17954.
[7] M.Y. Han, B. Özyilmaz, Y. Zhang, P. Kim, Phys. Rev. Lett. 98 (2007) 206805.
[8] D.V. Kosynkin, A.L. Higginbotham, A. Sinitskii, J.R. Lomeda, A. Dimiev, B.K. Price, J.M. Tour, Nature (London) 458 (2009) 872.
[9] L. Jiao, L. Zhang, X. Wang, G. Diankov, H. Dai, Nature (London) 458 (2009) 877.
[10] A.G. Cano-Márquez, F.J. Rodríguez-Macas, J. Campos-Delgado, C.G. Espinosa-González, F. Tristán-López, D. Ramírez-González, D.A. Cullen, D.J. Smith, M. Terrones, Y.I. Vega-Cantu, Nano Lett. 9 (2009) 1527.
[11] E.T. Mickelson, C.B. Huffman, A.G. Rinzler, R.E. Smalley, J.L. Margrave, Chem. Phys. Lett. 296 (1998) 188.
[12] K.F. Kelly, I.W. Chiang, E.T. Mickelson, R.H. Hauge, J.L. Margrave, X. Wang, G.E. Scuseria, C. Radloff, N.J. Halas, Chem. Phys. Lett. 313 (1999) 445.
[13] E.T. Mickelson, I.W. Chiang, J.L. Zimmerman, P.J. Boul, J. Lozano, J. Liu, R.E. Smalley, R.H. Hauge, J.L. Margrave, J. Phys. Chem. B 103 (1999) 4318.
[14] B. Huang, Y.-W. Son, G. Kim, W. Duan, J. Ihm, J. Am. Chem. Soc. 131 (2009) 17919.
[15] Y. Li, W. Zhou, H. Wang, L. Xie, Y. Liang, F. Wei, J.-C. Idrobo, S.J. Pennycook, H. Dai, Nat. Nanotech. 7 (2012) 394.
[16] D.M. Ceperley, B.J. Alder, Phys. Rev. Lett. 45 (1980) 566.
[17] T. Ozaki, H. Kino, Phys. Rev. B 69 (2004) 195113.
[18] N. Troullier, J.L. Martins, Phys. Rev. B 43 (1991) 1993.
[19] S.G. Louie, S. Froyen, M.L. Cohen, Phys. Rev. B 26 (1982) 1738.
[20] The Web Site of the OpenMX Package, ⟨http://www.openmx-square.org/⟩.
[21] H.J. Monkhorst, J.D. Pack, Phys. Rev. B 13 (1976) 5188.
[22] N.L. Rangel, J.C. Sotelo, J.M. Seminario, J. Chem. Phys. 131 (2009) 031105.
[23] M. Wu, J.S. Tse, J.Z. Jiang, J. Phys. Chem. Lett. 1 (2010) 1394.